AGU PUBLICATIONS

JGR

Journal of Geophysical Research: Solid Earth

RESEARCH ARTICLE

10.1002/2014JB011457

Key Points:
- Unprecedented systematic analysis of low-frequency earthquakes
- Precise details of two different low-frequency earthquake activity regimes
- Evolution of low-frequency earthquake activity during a strong slow-slip event

Correspondence to:
W. B. Frank,
frank@ipgp.fr

Citation:
Frank, W. B., N. M. Shapiro, A. L. Husker, V. Kostoglodov, A. Romanenko, and M. Campillo (2014), Using systematically characterized low-frequency earthquakes as a fault probe in Guerrero, Mexico, *J. Geophys. Res. Solid Earth*, *119*, doi:10.1002/2014JB011457.

Received 14 JUL 2014
Accepted 17 SEP 2014
Accepted article online 20 SEP 2014

Using systematically characterized low-frequency earthquakes as a fault probe in Guerrero, Mexico

William B. Frank[1], Nikolaï M. Shapiro[1], Allen L. Husker[2], Vladimir Kostoglodov[2], Alexey Romanenko[3], and Michel Campillo[4]

[1]Équipe de Sismologie, Institut de Physique du Globe de Paris, Paris Sorbonne Cité, CNRS, Paris, France, [2]Instituto de Geofísica, Universidad Nacional Autónoma de México, Mexico City, Mexico, [3]Department of Information Technology, Novosibirsk State University, Novosibirsk, Russia, [4]Institut des Sciences de la Terre, Université Joseph Fourier, CNRS, IRD, Grenoble, France

Abstract Studies of low-frequency earthquakes (LFEs) have focused on detecting events within previously identified tectonic tremor. However, the principal LFE detection tools of matched-filter searches are intrinsically incapable of detecting events that have not already been characterized previously as a template event. In this study, we therefore focus on generating the largest number possible of LFE templates by uniformly applying a recently developed LFE template detection method to a 2.5 yearlong data set in Guerrero, Mexico. Using each of the detected templates in a matched-filter search, we then form event families that each represents a single source. We finally develop simple, empirical statistics to select the event families that represent LFEs. Our resulting catalog contains 1120 unique LFE sources and a total of 1,849,486 detected LFEs over the 2.5 yearlong data set. The locations of the LFE sources are then divided into subcatalogs based on their distance from the subduction trench. Considering each LFE as a small unit of slip along the subduction interface, we observe discrete episodes of LFE activity in the region associated with large slow-slip events; this is in direct contrast to the near-continuous activity observed 35 km farther downdip within the previously identified LFE/tremor sweet spot.

1. Introduction

Low-frequency earthquakes (LFEs) are one of several recently discovered phenomena, along with tectonic tremor and slow-slip events (SSEs), that have been termed slow earthquakes [e.g., *Schwartz and Rokosky*, 2007; *Beroza and Ide*, 2011]. The principal feature of LFEs is their repetitive nature: each LFE source in space generates many events in time, called multiplets. Given the same source, path, and recording station, each LFE multiplet from a single source is characterized by the same waveforms. The first observations of LFEs in the context of slow earthquakes were made in the southwestern Japanese subduction zone within tremor, a long-duration (minutes to hours long) emergent seismic signal [*Shelly et al.*, 2006]. Tremors have since been suggested to be nothing more than a burst of LFEs [*Shelly et al.*, 2007a]. More recently, LFEs have also been observed in four other subduction zones: Costa Rica [*Brown et al.*, 2009], Cascadia [*Brown et al.*, 2009; *Bostock et al.*, 2012], Alaska [*Brown et al.*, 2013], and Mexico [*Frank et al.*, 2013]. In addition to subduction zones, LFEs have also been observed along the San Andreas Fault [*Shelly*, 2009] as well in New Zealand [*Chamberlain et al.*, 2014] and Taiwan [*Tang et al.*, 2010]. The emergent nature of a tremor makes it difficult to characterize, and LFEs, being much shorter-duration impulsive events, are often used as a proxy signal to characterize tremor [e.g., *Shelly et al.*, 2007b].

Despite being more easily characterized than tremor, LFEs present their own set of obstacles to overcome, namely, small signal-to-noise ratios (SNRs) that make detection difficult. Consequently, much of the investigation into LFEs has been dedicated to the development of the complex data analysis workflows necessary to detect, catalog, and characterize LFEs. The general LFE detection workflow is decomposed into two principal steps: (1) the detection of template LFEs, where each template represents a different LFE source, to be used in (2) the detection of the templates' multiplets through matched-filter searches. The matched-filter search is an incredibly powerful tool to detect events, even in very noisy environments; however, its intrinsic disadvantage is that it can only detect the multiplets of the LFE that was used, thereby eliminating the possibility of observing other sources. To generate a rich catalog of LFEs containing a maximum number of sources, it is therefore necessary to systematically search for LFE templates, just as matched-filter searches are used to systematically search for LFE multiplets.

Past studies have generated their catalogs of LFE templates in a variety of ways: through preexisting catalogs [*Shelly et al.*, 2006], through visual inspection [*Shelly*, 2009; *Tang et al.*, 2010; *Frank et al.*, 2013; *Chamberlain et al.*, 2014], or with automatic algorithms applied to previously identified tremor [*Brown et al.*, 2008, 2009, 2013; *Bostock et al.*, 2012; *Royer and Bostock*, 2013; *Frank and Shapiro*, 2014]. No study yet, however, has systematically analyzed a long, continuous data set for LFE templates, thereby maximizing the potential source coverage of the catalog resulting from the matched-filter search. Not taking into account visual inspection, which is both inefficient and suffers from the subjective perspective of the analyst, this is due to the fact that the principal automatic LFE template detection algorithm is computationally costly, with computational cost increasing nonlinearly as the analyzed time period increases [*Brown et al.*, 2008]. We attempt to address this lack of systematic LFE analysis with a study of slow earthquakes in the subduction zone in Guerrero, Mexico.

The subducting Cocos plate underneath Guerrero, Mexico, presents a unique subduction geometry that facilitates the observation of slow earthquakes for several reasons. Downdip of the seismogenic zone in the frictional transition zone, the subduction interface stays nearly horizontal for over 150 km at only ~45 km depth minimizing observation distance, as shown in Figure 1 [*Pérez-Campos et al.*, 2008; *Kim et al.*, 2010]. Multiple slow earthquake phenomena have been observed within the frictional transition zone along the horizontal portion of the subducting slab [*Larson et al.*, 2007; *Payero et al.*, 2008; *Frank et al.*, 2013]. For SSEs, the greatest concentration of displacement has been located just downdip of the seismogenic zone [*Radiguet et al.*, 2011]. Tremor on the other hand, has been observed to occur in two distinct regions, each with their own activity regime: (1) temporally coincident with SSEs at the downdip extent of the SSE source region around the first slab kink; (2) near continuously in a "sweet spot," ~50 km farther downdip than (1) [*Kostoglodov et al.*, 2010; *Husker et al.*, 2012]. Observations of LFEs so far have only been made within the sweet spot, where 29 sources have been shown to represent small shear slip events that release tectonic stress on the subduction interface [*Frank et al.*, 2013; *Frank and Shapiro*, 2014]. The combined Mexican LFE catalog from *Frank et al.* [2013] and *Frank and Shapiro* [2014], however, is far from exhaustive and only analyzed a small portion of the regional LFE activity.

Expanding on the previous work of *Frank et al.* [2013], we implement the LFE template detection algorithm of *Frank and Shapiro* [2014] to a continuous 2.5 year data set to extract a significant number of new sources and generate a new Mexican LFE catalog. We first will describe the method we applied to generate the catalog. We will then analyze the spatial and temporal distribution of LFEs in Guerrero, Mexico, and how it compares to previously identified tremor and SSEs.

2. Data

We use here the Meso-America Subduction Experiment (MASE) data set, a dense (5–6 km spacing), linear network of broadband seismic stations between Acapulco and Tempoal (running through Mexico City) that recorded at 100 Hz for 2.5 years [*Caltech*, 2007]. Ten stations (out of 100 total) were chosen for this study based on their relatively high SNRs, their proximity to the region of interest, and their availability or uptime; the geometry of the 10 station subnetwork is shown in Figure 1. The MASE network was operational between 1 January 2005 and 15 April 2007. Unless otherwise mentioned, the preprocessing we apply to the MASE data set is as follows: we first remove the daily mean and linear trend; we then apply a 1–2 Hz band-pass filter. This frequency band was chosen due to the nearly monochromatic nature of LFEs in Mexico [*Frank et al.*, 2013].

3. Method

We divide our detection workflow into two separate parts: (1) template detection and (2) multiplet detection. Each template and its detected multiplets form an event family that is defined by two observables: (1) its catalog of detection times and (2) the stack of all of the multiplet waveforms, which results in high-quality waveforms with visible phases. We remove event families that do not resemble LFEs and combine any LFE families that most likely originate from the same source. We then go through our detection workflow one more time using the stacks of the remaining LFE families as templates for new LFE families. After the second iteration of the detection workflow, we once again remove any poor-quality event families, regroup any redundant families, and finally locate each of the remaining robust LFE families. We will now describe in more detail each of these steps in the following subsections.

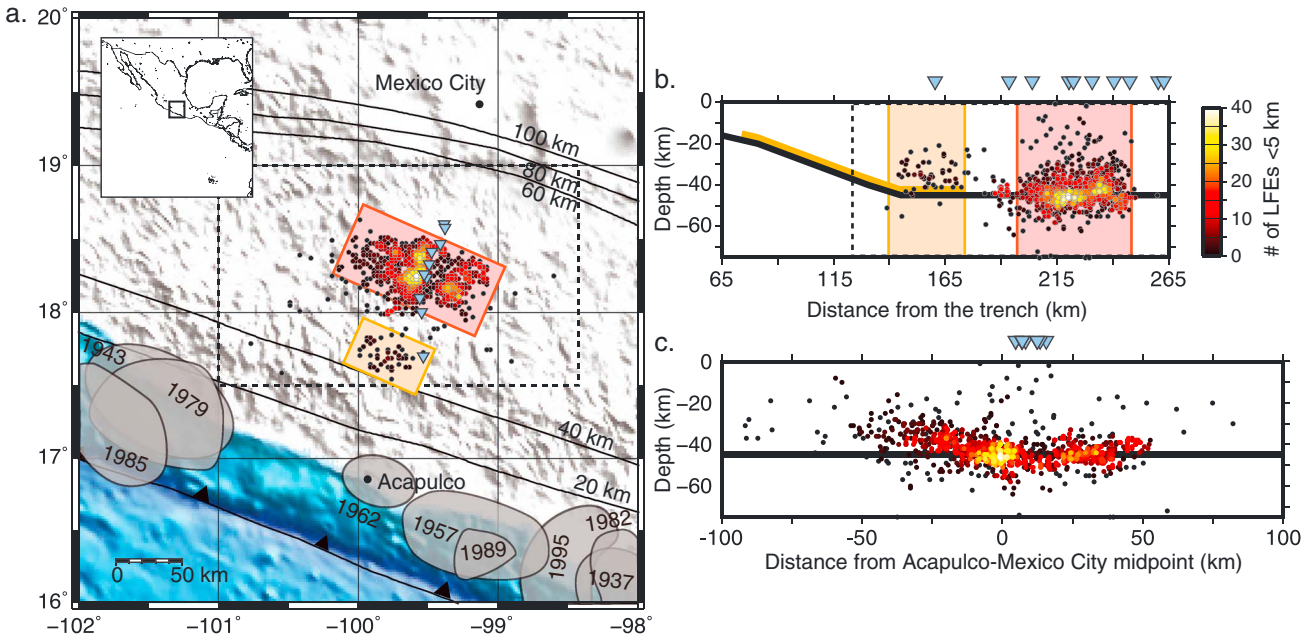

Figure 1. (a–c) Horizontal and vertical slices of LFEs in the Guerrero, Mexico, study area. The map inset shows this study's region of interest. The 1120 LFEs characterized in this study are plotted as points; their color represents the location density, calculated for each LFE family as the number of other LFEs closer than 5 km. The 10 MASE stations that were used in this study are shown by the blue inverted triangles in Figures 1a and 1b. The red and yellow boxes in Figures 1a and 1b indicate the two LFE-active source regions: the yellow box is the region that was active during the large 2006 slow-slip event and is referred to as the transient zone; the red box is the LFE/tremor sweet spot, where near-continuous LFE and tremor activity is observed. The solid black lines in Figures 1a–1c represent the subducting Cocos plate geometry [*Kim et al.*, 2010]. The vertical profile between Acapulco and Mexico City is plotted in Figure 1b; the vertical profile perpendicular to Figure 1b is plotted. Historical earthquakes (with rupture years) highlighting the Guerrero seismic gap are indicated by the grey shaded patches (from *Kostoglodov and Pacheco* [1999], http://usuarios.geofisica.unam.mx/vladimir/sismos/100a%F1os.html) (Figure 1a). The thick yellow band above the subduction interface shows the calculated slip that occurred during the 2006 slow-slip event [*Kostoglodov et al.*, 2010] (Figure 1b). Vertical profile perpendicular to the midpoint of Figure 1b (Figure 1c). The horizontal axis is exaggerated.

3.1. Template Detection

We use the event detection method proposed by *Frank and Shapiro* [2014], called the beamformed network response. The method consists of searching through a data set for seismic energy that originates from a predefined source location. We use the same grid of potential sources as *Frank and Shapiro* [2014] that is focused on the LFE/tremor-active region: a 3- D grid with dimensions of 100 by 100 by 75 sources in latitude, longitude, and depth, respectively; the longitude grid interval is 0.025° or ~3 km, the latitude grid interval is 0.02° or ~2 km, and the depth grid interval is 1 km. We use the regional *S* wave velocity model of *Iglesias et al.* [2010] to calculate the *S* wave traveltimes from each of the theoretical sources on the 3-D grid to the 10 MASE stations with a ray tracing technique. We only use *S* wave traveltimes as the *P* waves of LFEs are frequently below the noise level of the MASE network [*Frank et al.*, 2013]. For each of the calculated relative *S* wave moveouts, we then align and sum the instantaneous seismic energy of the entire data set. The aligned and summed seismograms represent the beamformed network responses of the data set to each of the potential sources in the chosen 3-D grid. So that no one station will dominate the network response, we first normalize the waveforms by the RMS for each station and component. We represent the beamformed network response, NR, mathematically as follows:

$$\mathrm{NR}(t,\phi,\lambda,z) = \sum_i \frac{s_i'(t,\phi,\lambda,z)^2}{\sqrt{N^{-1}\sum_n^N s_i'(t+n\Delta t)^2}}, \tag{1}$$

where t is time, n is the discrete sample; N is the total number of samples; Δt is the constant time step; (ϕ, λ, z) are, respectively, latitude, longitude, and depth; and $s_i'(t,\phi,\lambda,z)$ is the seismogram recorded at the ith station that has been aligned with the relative *S* wave moveout predicted by a theoretical point source located at (ϕ, λ, z). We note that we only use the *N-S* component of the 10 MASE stations as the strongest LFE ground motions have been observed on the horizontal components [e.g., *Shelly et al.*, 2006; *Payero et al.*, 2008; *Frank et al.*, 2013].

A peak in the beamformed network response for a given potential source indicates a moment in time when the network observes energy originating from that source; a potential template event is then picked as the 8 s long time window centered on the beamformed network response peaks with the same moveout as that potential source. The time window length of 8 s was chosen as a compromise to ensure that as much of the signal is captured within the window while limiting the amount of noise within the template waveforms. To ensure that we do not use random noise as a template event, we calculate the coherence, C, of the potential template signal across the network as described by *Frank and Shapiro* [2014]. This consists of calculating the average absolute value of the correlation coefficients between every unique pair of stations in the network within the potential template's time window, as shown here:

$$C = \frac{\sum_{i_{kl}=1}^{\frac{I(I-1)}{2}} \left| \left\langle s'_k(t,\phi,\lambda,z), s'_l(t,\phi,\lambda,z) \right\rangle_{i_{kl}} \right|}{I}, \tag{2}$$

where i_{kl} is the ith unique combination of station k and station l, I is the total number of stations, and $\left\langle s'_k(t,\phi,\lambda,z), s'_l(t,\phi,\lambda,z) \right\rangle_{i_{kl}}$ is the correlation coefficient between the pair of aligned seismograms at stations k and l. *Frank and Shapiro* [2014] used a coherence threshold of 0.2; we use here instead a dynamic threshold that depends on the number of functioning stations at any given time. We detail the dynamic threshold we used in the later section on data continuity. We then use each of the chosen event templates in a matched-filter search to detect its multiplets. We note that although we use all 10 of the selected MASE stations for the template detection, we only use the five stations that record the highest amplitudes for each of the template events for the following matched-filter search to reduce the computational cost.

3.2. Multiplet Detection

The matched-filter search we use to detect multiplets [*Gibbons and Ringdal*, 2006] has become the standard way to compile LFE families [*Shelly et al.*, 2006; *Shelly*, 2009; *Brown et al.*, 2009, 2013; *Bostock et al.*, 2012; *Frank et al.*, 2013; *Royer and Bostock*, 2013]. We search for other events that are very similar to the template by correlating the data set in a sliding time window that preserves the template's moveout with the template itself. For each sliding window, the correlation coefficients across the network are summed and if the sum is above some detection threshold, then that sliding window contains a multiplet of the template event. We note that all three station components are used to calculate the correlation coefficients. We represent the correlation coefficient sum as a function of time, $\mathrm{CS}(t)$ in the following manner:

$$\mathrm{CS}(t) = \sum_{i}^{I} \sum_{j}^{J} \frac{\sum_{n}^{N} \tau_i^j(n\Delta t) s_i^j(t + \delta_i + n\Delta t)}{\sqrt{\sum_{n}^{N} \tau_i^j(n\Delta t)^2 \sum_{n}^{N} s_i^j(t + \delta_i + n\Delta t)^2}}, \tag{3}$$

where j represents the component, J is the total number of components, $s(t)$ is the discrete seismic signal, $\tau(t)$ is the template LFE recorded in relative time starting at $t = 0$, and δ_i is the time delay at station i relative to the template's first arrival. The detection threshold that we use in this study is further discussed in the following section.

We evaluate the robustness of the detected multiplets using the method of *Frank et al.* [2013]. Once the robust multiplets of an LFE family are determined, we then stack their waveforms together to produce high SNR waveforms representative of the LFE family and its source.

3.3. Detection Thresholds and Data Continuity

When systematically analyzing a continuous data set, the uptime of the network plays an important role in interpreting the resulting catalog. One must take special care to ensure that the detection capability of the applied methods is continuous over the entire data set, despite an evolving network uptime due to station outages or other gaps in the data. We therefore adapt our detection thresholds to the network continuity for both template and multiplet detections. For each step, we will first describe how a station outage or a gap in the data affects the detection criteria and then describe our solution.

After determining peaks in the beamformed network response as local maxima (and therefore not subject to a threshold), we calculate the coherence of the waveforms centered on each peak as described in a previous section. As the number of functioning stations decreases, there is a greater and greater chance that the remaining waveforms resemble one another and that the coherence is larger; i.e., the chance that two monochromatic sinusoids are in phase and strongly correlated is greater than the chance that 10 monochromatic sinusoids are all in phase and are strongly correlated. We first adopt a base coherence threshold

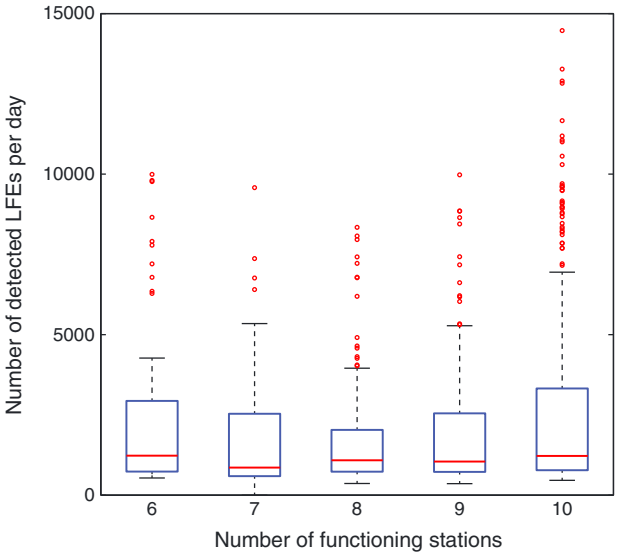

Figure 2. Number of LFE detections per day as a function of functioning stations. Each box and whiskers plot represents the days of the MASE deployment that had the corresponding number of functioning stations. The blue box represents the interquartile range (IQR) (25% quantile to 75% quantile). The red line represents the median. The whiskers extend to ±1.5 IQR. The red circles represent any outliers farther than the whiskers.

of 0.3 that is more selective than the 0.2 coherence threshold used in [*Frank and Shapiro*, 2014]. We then empirically modulate the coherence threshold, C', by the number of functioning stations as follows:

$$C' = \frac{0.3}{\frac{I_f}{I}}, \tag{4}$$

where I_f is the number of functioning stations. Despite a normalization of the coherence, there will always be a greater uncertainty of the templates detected during station outages given that there is less available data to analyze. Our goal, therefore, was not to obtain a uniform detection rate over the data set but to instead favor template detection when the network was fully functional over periods of station outages. Without this normalization, we found an abundance of detected templates when $I_f < I$, which is what one would expect given a greater chance of having a high coherence with fewer functioning stations. Afterward, however, the template detection rate was greater when the network was fully functioning, while still allowing detections during station outages.

The situation is similar for the multiplet detection: our detection criteria depends once again upon the sum of a quantity, correlation coefficients in this case, over the network. If there are missing stations on certain days, the correlation coefficient sum would not be uniformly calculated over the network deployment. Similar to the previous solution, we therefore modify our detection threshold based on the number of operating stations on any given day. We use a dynamic threshold of 5 times the daily RMS of the correlation coefficient sum, similar to *Frank et al.* [2013]:

$$T = 5\sqrt{\frac{\sum_n^N \mathrm{CS}\,(t + n\Delta t)^2}{N}}, \tag{5}$$

where T is the detection threshold. This proved to provide a uniform number of detections per day. Figure 2 shows that a significant majority (within the interquartile range of 25% to 75% quantiles) of analyzed days in the final catalog yielded a consistent number of detections per day using the above dynamic threshold, regardless of the number of functioning stations.

3.4. Selecting LFE Families

Our template detection method combined with the multiplet detection generates an enormous amount of events that can contain event families that do not robustly stack, perhaps due to a random noise event being used as a template, event families that are not LFEs, and LFE families that represent the same source. Based on previous observations of LFEs [*Frank et al.*, 2013; *Frank and Shapiro*, 2014], we identify LFEs as short-duration impulsive events that occur in swarms or bursts. We therefore developed two simple empirical statistics to select the robust LFEs among all of the event families and to combine any redundant families together.

3.4.1. Robust LFE Selection

A poor-quality event family is distinguishable in two ways. The first is that its multiplets are randomly distributed in time and do not occur in swarms or bursts of activity similar to LFEs [*Shelly*, 2010]. A clear comparison of this is shown in Figures 3a and 3c. A second is that the stacked waveforms of a poor-quality family will not reveal *P* waves. This will not be the case for a robust LFE family's stacked waveforms, as demonstrated by the clear *P* waves in Figure 3b.

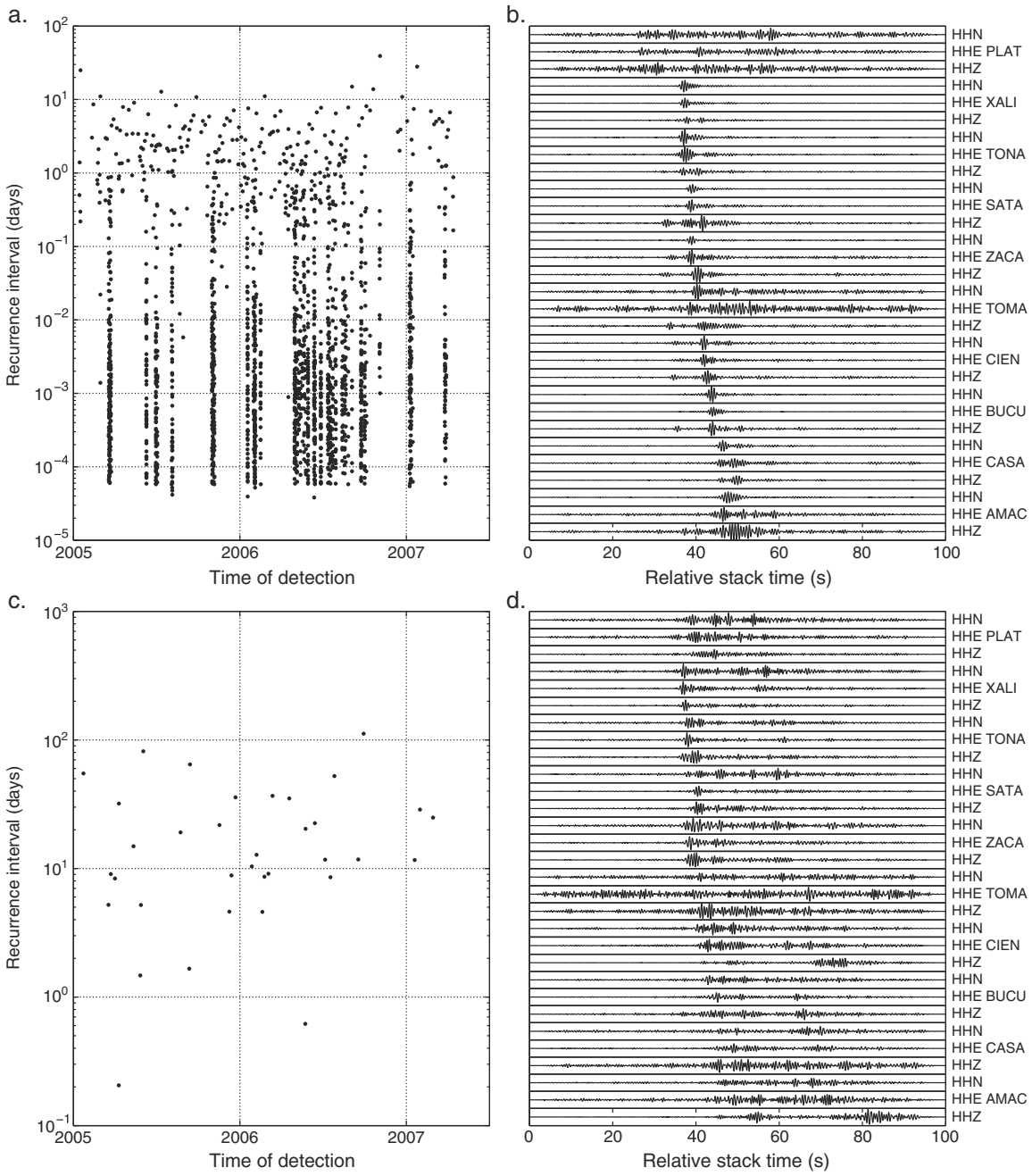

Figure 3. Recurrence intervals and stacked waveforms for both (a and b) a robust LFE family and (c and d) a poor-quality event family. The robust LFE family contains 2184 multiplets, while the poor-quality event family contains only 26 multiplets. The recurrence intervals plotted in Figures 3a and 3c represent the elapsed time between consecutively detected multiplets. The stacked waveforms in Figures 3b and 3d are the normalized sum of all of the families' respective multiplets. Note the clear *P* and *S* wave arrivals in Figure 3b and the long emergent waveforms in Figure 3d.

To therefore evaluate whether an event family is an LFE, we calculate the percentage of multiplets in each LFE family that occur less than 10 min apart from each other; we call this the family burstiness. When the burstiness is small enough, the LFE family's multiplets no longer occur in bursts and are more or less randomly distributed in time. We determined an empiric threshold of 5% after examining the distribution of family burstiness and the stacked waveforms of the highly random LFE families; all families below the threshold were considered random noise families and removed.

3.4.2. Regrouping Redundant LFE Families

It is necessary to check the redundancy of LFE families given that the template detection method could find two different events in time that originate from the same source, generating two LFE families that would be very similar. To determine if an LFE family is redundant, we first compare the detection times of one family, defined as a vector of detection times t_m with length M, to the detected multiplets of all other LFE families. Any multiplet that is detected within 5 s of another family's is considered to have been detected at the same time. The 5 s long slack allows for the fact that the start of the event's waveform within the 8 s long template is not necessarily at the same time for each template. We then calculate the percentage of multiplets of a family that are considered to have been detected at the same time as the events of another family; this statistic, which we call the family redundancy, R, is therefore defined for each unique pair of event families a and b:

$$R^{ab} = \frac{\sum_m^M r^b(t_m^a)}{M}, \tag{6}$$

where $r^b(t_m^a)$ is defined as

$$r^b\left(t_m^a\right) = \begin{cases} 1 & \text{if} \quad \min_{m'} |t_m^a - t_{m'}^b| \le 5 \\ 0 & \text{otherwise} \end{cases}, \tag{7}$$

where m' is the detection number of family b (of M' total). If this statistic is also greater than some threshold for a given pair of families, we then calculate the waveform similarity of the two families' stacked waveforms, $\mathrm{SW}_i^j(t)$ recorded in relative time starting at $t = 0$. We define the waveform similarity, S as the average of the correlation coefficients of the two LFE families a and b's stacked waveforms, calculated station by station, component by component. This is represented mathematically as

$$S = (IJ)^{-1} \sum_i^I \sum_j^J \frac{\sum_n^{N_a} \mathrm{SW}_i^j(n\Delta t)^b \mathrm{SW}_i^j(n\Delta t)}{\sqrt{\sum_n^{N_a} \mathrm{SW}_i^j(n\Delta t)^2 \sum_n^{N_b} \mathrm{SW}_i^j(n\Delta t)^2}}. \tag{8}$$

If the waveform similarity is greater than some threshold, the event families are considered redundant and their multiplets are combined into a new family. We found that setting the redundancy and waveform similarity thresholds to 0.5 actually changed the SNR of the resulting combined family's stacked waveforms by −2%, indicating that the LFE families are not similar enough to constructively stack. We therefore used a stricter threshold of $\frac{2}{3}$ for both the redundancy and the waveform similarity that increased the mean stack SNR by 1% while combining 2629 event families together into 1068 event families in the final catalog.

3.5. Second Iteration With Stacked Waveform Templates

We are now left with the remaining robust LFE families. The stacked waveforms of each family have larger SNRs than the original template event used to generate that family. Following *Frank et al.* [2013], we generate a new template for each robust family using a 16 s long time window centered on the arrivals within the stacked waveforms. The entire process outlined in the previous sections is then repeated a second time using the new and improved template derived from the stacked waveforms that generates a larger family of multiplets thanks to its increased SNR.

Despite the two empirical statistics that are used to select robust LFE families, there are still a number of them that have poor-quality stacked waveforms that remain after the second iteration. We calculate the SNR of each of the remaining families' stacked waveforms in the following manner:

$$\mathrm{SNR} = \mathrm{median}_{ij}\left[\frac{\max_t \mathrm{SW}_i^j(t)}{\sqrt{N^{-1}\sum_n^N \mathrm{SW}_i^j(n\Delta t)^2}}\right]. \tag{9}$$

Similar to the previous two empirical statistics, after investigating the quality of the stacked waveforms for a variety of SNRs, we apply a threshold to remove the lowest third of observed SNRs. The robust LFE families at the end of this process are then considered to be the comprehensive catalog of LFEs in our study region of Guerrero, Mexico.

3.6. Automatic Source Location

Frank and Shapiro [2014] stated that the beamformed network response could be used to automatically locate LFEs, but because only *S* waves were used, the locations would be poorly constrained, notably in depth. This location is more accurate, however, if used on the stacked waveforms of the robust LFE families whose *P* waves have emerged after stacking the family's multiplets. Therefore, the beamformed network response of each robust LFE family can be calculated using the same 3-D grid of potential sources as the template detection described earlier, but this time also incorporating the *P* wave along with the *S* wave. In practice, we sum together the beamformed network response to both the *P* wave moveout and the *S* wave moveout. To ensure that the two network responses will constructively stack at the same first arrival, we modify the *S* wave moveout to be relative to the first *P* wave arrival instead of the first *S* wave arrival. Slightly modifying equation (1), we represent the *P* and *S* wave beamformed network response as follows:

$$\mathrm{NR}^{P+S}(t,\phi,\lambda,z) = \mathrm{NR}^{P_P}(t,\phi,\lambda,z) + \mathrm{NR}^{S_P}(t,\phi,\lambda,z), \tag{10}$$

where $\mathrm{NR}^{P_P}(t,\phi,\lambda,z)$ is the beamformed network response to the *P* wave originating from a source located at (t,ϕ,λ,z) and $\mathrm{NR}^{S_P}(t,\phi,\lambda,z)$ is the beamformed network response to the *S* wave originating from the same source relative to the first arriving *P* wave. We note that using this new notation, the left-hand side of equation (1) could be rewritten as $\mathrm{NR}^{S_S}(t,\phi,\lambda,z)$. The potential source that generates the largest beamformed network response is then used as the most likely location of that LFE family's source. Unlike the template detection step, we initially calculate the network response without normalizing the seismograms by their RMS.

Not all LFE families will, however, stack evenly and at the same rate across all stations, resulting in stacked waveforms with large differences in amplitude across the network. This can reduce the quality of the location because some stations carry more weight when calculating the network response. We resolve this issue by normalizing the stacked waveforms by station and component before locating the LFE family.

4. Results

Our final catalog of LFEs contains 1120 families with a total of 1849486 multiplets detected over the 2.5 year MASE deployment; we observe an average of about 2000 LFEs per day. We will now go through each of the major catalog aspects in detail.

4.1. LFE Locations

As shown in Figure 1, the LFE family locations are grouped along the subduction interface, with the largest concentration of LFEs within the sweet spot [*Husker et al.*, 2012; *Frank et al.*, 2013]. There are, however, several outliers either close to the surface or deep beneath the plate interface. These sources had smaller numbers of multiplets than the other robust LFEs and the relatively lower SNRs of the stacked waveforms are closer to the threshold described above. We decided, however, to include these families because their activity in time strongly resembled the more robust LFE sources. In Figure 1c, we observe a banana-shaped distribution in longitude that reflects the uncertainty due to the linear network geometry. This could explain the shallow depths of the outliers as they are located on the extreme edge of the banana-like distribution; we consider, however, their along-dip location robust with an uncertainty of less than 5 km.

In addition to a large concentration of LFEs within the sweet spot, we were also able to detect 52 LFE families within the region farther updip that has been associated with large SSEs and where tremor has been observed to occur during large SSEs [*Kostoglodov et al.*, 2010]. For brevity and clarity's sake, we will refer to the portion of the subduction interface between 205 and 250 km from the trench as the sweet spot (the red patch in Figure 1b) and the portion of the subduction interface between 140 and 170 km as the transient zone (the yellow patch in Figure 1b). We refer to the region between the sweet spot and the transient zone as the buffer zone. The extent of the sweet spot as we observe it reaches 10 km farther updip than the sweet spot defined by *Husker et al.* [2012]. This is not due to a change in the definition of the sweet spot but is instead due to a greater number of located sources that exhibit near-continuous activity.

As can be seen in Figure 1b, the slip that occurred during the 2006 SSE extends much farther updip than the temporally correlated transient LFE sources shown in Figure 5. A similar spatial limit has also been reported for tremor [*Kostoglodov et al.*, 2010; *Husker et al.*, 2012]. We note that the greatest concentration of slip during the 2006 SSE was also located farther updip than any tremor or LFE activity, suggesting that SSEs and

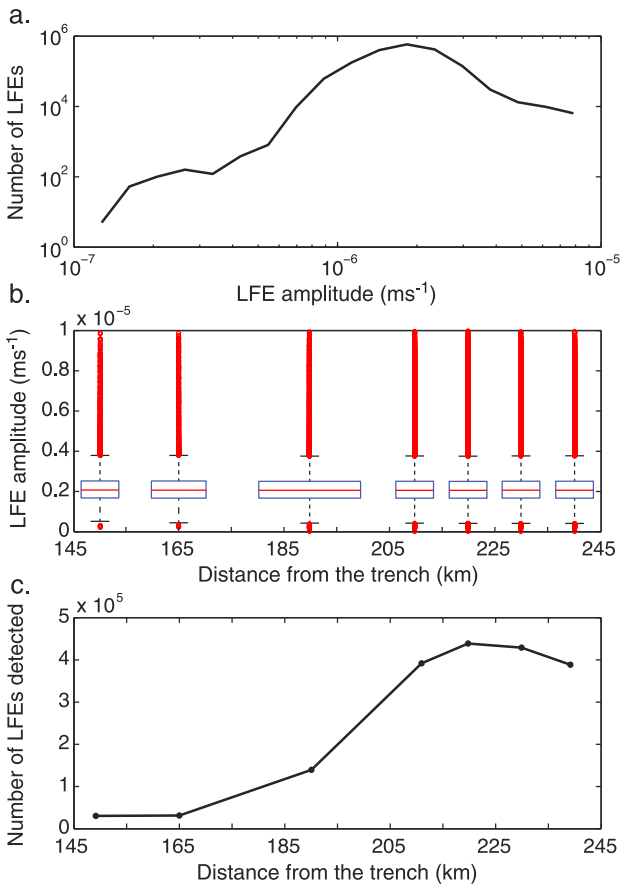

Figure 4. Distribution of LFEs and their amplitudes along the subduction interface. (a) The amplitude distribution for the entire LFE catalog; (b) the amplitude distribution with respect to distance from the trench. (c) The total number of LFEs detected along dip. In Figure 4b the blue box represents the interquartile range (IQR) (25% quantile to 75% quantile). The red line represents the median. The whiskers extend to ±1.5 IQR. The red circles represent any outliers farther than the whiskers. We note that the >3000 outliers in each subcatalog only represent on average 2.5% of the total LFEs in that subcatalog.

LFEs/tremor are distinct phenomena and do not have the same source [*Radiguet et al.*, 2011]. The detection of the transient zone LFEs is most likely due to the systematic search implemented in this study; *Frank et al.* [2013] posited that LFEs should exist in the transient zone but did not observe any after a visual inspection of the data set. The locations of the transient zone LFEs are more dispersed in depth than the sweet spot LFEs, but this is most likely due to the choice of the MASE subnetwork and uncertainty associated with the simplified plate geometry used [*Kim et al.*, 2010]. The station coverage above the transient zone is much sparser than that above the sweet spot, increasing the uncertainty in depth. We also note a lack of LFEs around 175 km from the trench in the buffer zone, between the transient zone and the sweet spot. We suggest that the lack of LFEs reflects the evolution of the frictional conditions that separate the transient zone from the sweet spot.

We picked amplitudes for each of the detected LFE multiplets. Given the catalog's proximity to the MASE network, we did not apply any attenuation or geometrical spreading corrections. Instead, we first measured the maximum amplitude of each station and component within the LFE multiplet's detection window. To then reduce the influence of any spurious spikes within the data, we determined the LFE's amplitude to be the median of all of the measured max amplitudes. The amplitude distribution for the entire LFE catalog, shown in Figure 4a, cannot be fitted by a Gutenberg-Richter law and instead reflects a characteristic amplitude, similar to what has been observed in Japan and New Zealand [*Aso et al.*, 2013; *Chamberlain et al.*, 2014]. With respect to distance from the trench, the distribution of LFE amplitudes is remarkably uniform, about a micrometer per second, despite a significant difference in the amount of LFEs detected (Figures 4b and 4c).

4.2. LFE Activity in Time and Space

As each LFE family represents a single source, we attribute the same location to each of the LFE multiplets in a given family. The locations in time and space of every LFE in the catalog can then be plotted to study the evolution of LFE activity. Figure 5 shows the LFE activity over the 2.5 yearlong MASE deployment for all 1120 LFE families. We first remark the sharp division between the edge of the sweet spot and the rest of the LFE source region farther updip: there is nearly continuous activity within the sweet spot, punctuated by multiple clusters of activity closely spaced in time that we will call LFE episodes. Updip of the sweet spot, however, there is a distinct decrease in the amount of interepisode activity. Dividing the LFE catalog into two subcatalogs, one for the sweet spot and one for the transient zone, we can represent the LFE activity in terms of recurrence intervals as shown in Figure 6. We define the LFE recurrence interval as the elapsed time between two sequential multiplets. The large LFE episodes are much more clearly identifiable in the

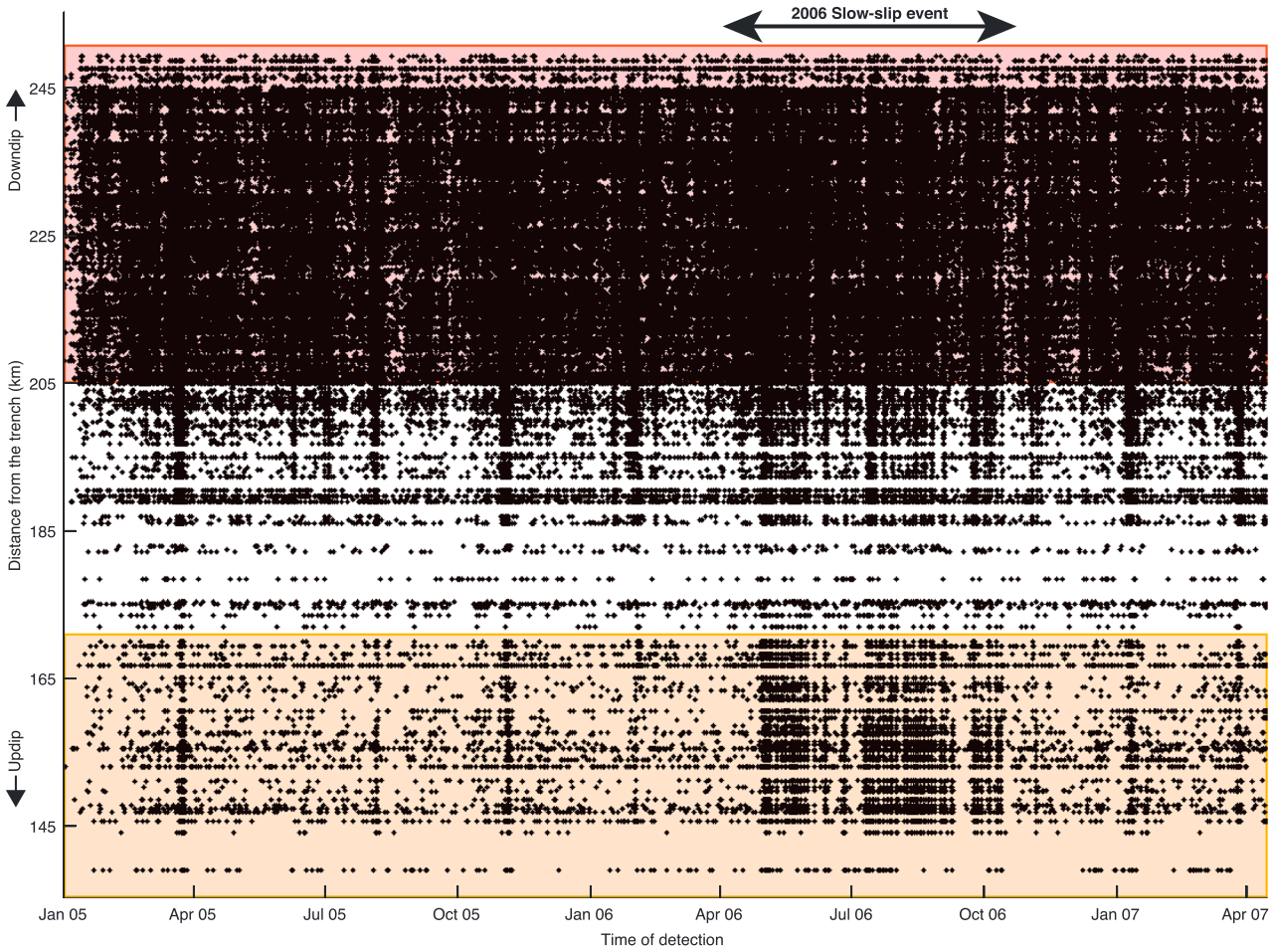

Figure 5. Complete Mexican LFE catalog in time and space. Each LFE family contains a number of multiplets that all have the same source as the LFE family's template; each LFE family therefore has a unique distance from the trench and can be found along a horizontal line with respect to the time of detection. To improve visibility, we only plot here the LFEs that have correlation coefficients greater than the median, which represents 50% of the total catalog of 1,849,486 multiplets. The colored regions represent the two LFE/tremor source regions shown in Figure 1: the yellow box is the region that was active during the large 2006 slow-slip event; the red box is the LFE/tremor sweet spot, where near-continuous LFE and tremor activity is observed. The time period of the 2006 SSE is shown by the black arrow.

transient zone subcatalog with recurrence intervals, as shown in Figure 6b. We identify six large LFE episodes within the catalog that do not accompany the 2006 SSE: March 2005, August 2005, November 2005, January 2006, January 2007, and March 2007. In the transient zone, apart from the LFE episodes, the defining feature is activity associated with the 2006 SSE from April 2006 to October 2006. If one were to only consider the sweet spot LFEs, however, SSE-associated increase of activity is nearly impossible to distinguish. We note that these six episodes are also well correlated in time with the tremor episodes identified by *Husker et al.* [2012], further evidence that LFEs and tremor are closely related.

4.3. LFE Episodes

If we focus on a single LFE episode of activity in late March 2005, as shown in Figure 7, the difference in LFE activity between the sweet spot and the buffer zone around 205 km from the trench is no longer evident and we can no longer distinguish a clear regime change between the two zones. The sweet spot and the buffer zone are dominated by clear migrations that move both downdip and updip but do not extend into the transient zone; given the linear network geometry, we are unfortunately unable to determine if the migration direction is parallel to the subduction rake. The apparent migration velocity measured in any given LFE episode is on the order of 30 km h^{-1} over 30–60 km, comparable to LFE and tremor migrations in Japan and Cascadia [*Shelly et al.*, 2007b; *Ghosh et al.*, 2010]. We did not perform any systematic analysis of LFE migrations, but we remark that clear migrations are rarely seen outside of LFE episodes. Migrations are observed primarily in the sweet spot and the buffer zone. We do not observe any migrations within the

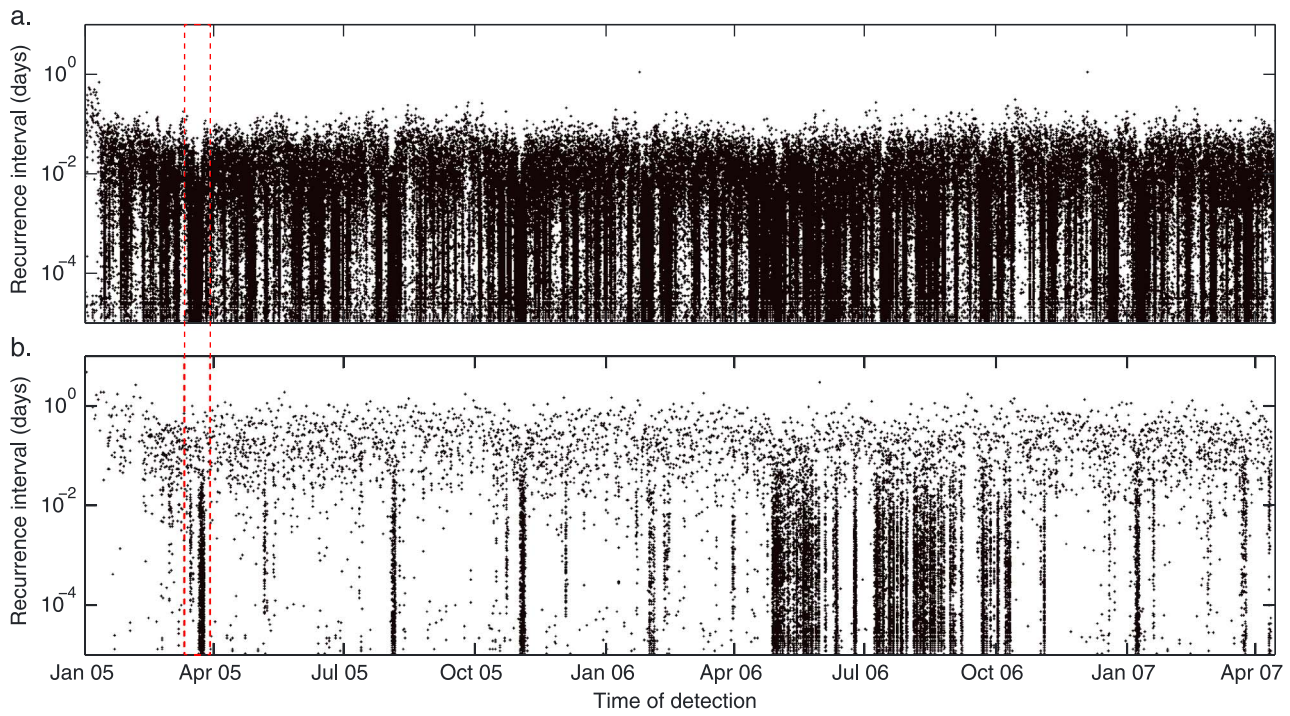

Figure 6. Recurrence intervals of the two principal LFE source regions. To improve visibility, we only plot here the LFEs that have correlation coefficients greater than the median, which represents 50% of the total catalog. The LFE episode shown in Figure 7 is indicated by the dashed red box. (a) Recurrence intervals of sweet spot LFEs, located farther away than 205 km from the trench. The principal observation is that the sweet spot activity occurs in clusters of events, represented here by vertical streaks. (b) Recurrence intervals of transient zone LFEs, located closer than 170 km to the trench. Once again, the LFE activity manifests in clusters of events spread over several days. More importantly, however, the large 2006 SSE, which occurred between April 2006 and November 2006, is extremely evident and is accompanied by increased LFE activity during its duration.

transient zone, but the smaller number of LFE sources in the transient zone most likely affects their visibility if they do occur. Additionally, like in Japan and Cascadia, LFE episodes frequently initiate downdip with an updip-migrating cluster of LFEs [*Obara et al.*, 2010; *Wech and Creager*, 2011]. If we now consider the entire LFE source region, activity within the sweet spot routinely starts 3–5 days before there is an abrupt increase in activity within the transient zone. This pattern of activity is a consistent feature of all of the six major LFE episodes.

4.4. Numerical Implementation

The numerical implementation of this systematic cataloging took full advantage of the inherent parallelism of the two detection algorithms. For the template detection, the large majority of the computational cost lies with the alignment and stacking of the continuous seismograms for each source of the 3-D grid. Each point source (and its associated moveout) is, however, completely independent of all other sources and can be calculated in parallel. The calculation of the correlation coefficients, a simple dot product, is the main bulk of the computations for the matched-filter search. Once again, however, the problem can be reduced into many small independent calculations: the correlation coefficient sum of each sliding window comparing the template event and the data set is fully independent. The architecture of graphics processing units (GPUs), compared to standard central processing units (CPUs), is specifically designed to handle thousands of simple calculations in parallel. Taking advantage of a small cluster of eight Nvidia Tesla K20 GPUs, each having 2496 computational cores, we were able to process the entire catalog of 1120 LFE families plus the spurious event families that were eventually removed in 8 days. Such rapid computation allows us to repeat the processing of the continuous data analysis to evaluate the effect of various parameters.

5. Discussion

Other LFE catalogs, have focused the LFE template detection step on previously observed tremor [e.g., *Brown et al.*, 2009; *Bostock et al.*, 2012]; here, however, the beamformed network response of *Frank and Shapiro* [2014] was applied continuously to a 2.5 year data set. The emphasis on the template detection

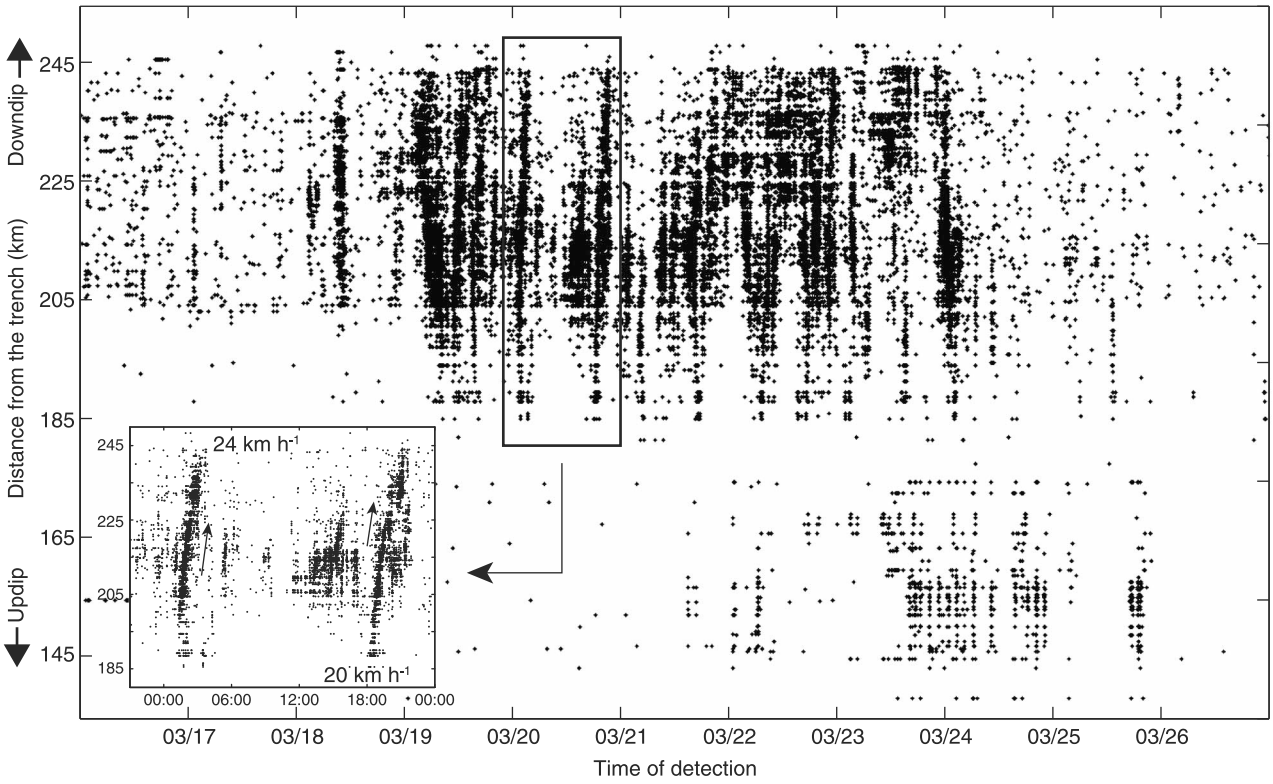

Figure 7. Evolution of an LFE episode in time and space. Each LFE family contains a number of multiplets that all have the same source as the LFE family's template; each LFE family therefore has a unique distance from the trench and can be found along a horizontal line with respect to the time of detection. The sweet spot is between 205 and 250 km from the trench; the transient zone is between 140 and 170 km from the trench; the buffer zone is the region between the transient zone and the sweet spot. The inset shows a zoom of two clear downdip migrating LFE bursts with their velocities indicated. The migration velocity of LFE clusters is typically on the order of 30 km h^{-1} over 30–60 km. We note the 4 day delay of the start of activity between the sweet spot and the transient zone. We also remark that the migrations observed in the sweet spot extend into the buffer zone during LFE episodes.

provided a great number of LFEs that were then used in a matched-filter search to detect nearly 2 million LFE multiplets. This extremely detailed catalog provides a clear picture of the activity along the subduction interface: we are able to provide more precise limits of the sweet spot and the transient zone than previous studies of Guerrero tremor and LFEs [*Husker et al.*, 2012; *Frank et al.*, 2013]. If we consider all of the 374 days during the MASE deployment when a LFE template was detected, tremor was only observed on 149, or 40%, of those days [*Husker et al.*, 2012]. We can therefore attribute a majority of the newly characterized LFE sources to the fact that the entire data set was systematically analyzed and that our study was not limited to analyzing tremor-active periods of time.

The close relationship between LFEs and tremor has long been suspected with tectonic tremors suggested to be made up of a swarm of LFEs [e.g., *Shelly et al.*, 2007a]. To evaluate this relationship in Guerrero, we perform a simple calculation to quantify the percentage of detected LFEs that occur during tremor. We find that only 18.3% of all LFEs occur during tectonic tremor using the most recent Guerrero tremor catalog [*Husker et al.*, 2012]. Although the tremor catalog is most likely missing a number of tremor events, there is still quite a significant number of LFEs that cannot be explained by tremor. If we instead consider the situation from the opposite angle so that the detection efficiency of tremors isn't taken into account, we find the percentage of tremors that are covered by LFEs to be 35.4% using an exaggerated LFE duration of 6 s. Regardless of whether we focus on the tremor catalog or the LFE catalog, the significant portion of the observed LFE activity in Guerrero that is not related to tremor leads us to suggest that the relationship of LFE and tremor is not as clear cut as previously suggested.

The sweet spot of the Mexican subduction has previously been suggested to have the necessary pressure/temperature conditions and fluid content to continuously generate tremor and LFE activity along the subduction interface [*Husker et al.*, 2012; *Frank et al.*, 2013]. Our observations of the same near-continuous activity confirm that the sweet spot LFE activity is significantly different from other LFE source regions

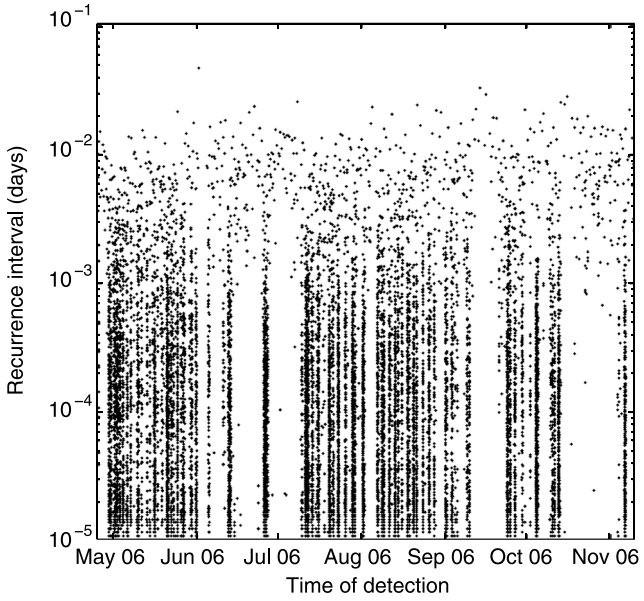

Figure 8. Recurrence intervals of the transient zone LFEs during the 2006 SSE. To improve visibility, we only plot here the LFEs that have correlation coefficients greater than the median, which represents 50% of the total catalog. The LFE activity during the SSE is not continuous but is instead separated into discrete clusters of events.

farther updip. Further proof of this is the large amount of activity in the sweet spot compared to the rest of the LFE source region, as shown in Figure 4c. Taking into account the locations of the continuously active LFE sources, we extend the updip limit of the sweet spot defined by *Husker et al.* [2012] by 10 km.

The more precise locations in space and time of LFEs compared to tremors have revealed migrations of activity moving updip and downdip in the sweet spot and the buffer zone. Observed migration speeds of 30 km h^{-1} are much more rapid than propagating SSE slip fronts and are similar to migrating tremors and LFEs in other slow earthquake regions [*Shelly et al.*, 2007b; *Ghosh et al.*, 2010]. The erratic evolution of LFE migrations indicates that slip is not released in a single, slow-slip event along the interface but is instead highly heterogenous. The migrations are most likely associated with an activity pattern resembling an avalanche where static and dynamic triggering following an initiating event increases the LFE activity until a peak, and activity then dies out after the accumulated tectonic stress is released across the activated heterogeneities. The mechanics of LFE migrations is an important piece of the slow earthquake puzzle and a quantitative study of the migrations observed here will most likely be undertaken in the future.

Our catalog provides the first observations of LFEs along the downdip extent of the subduction interface that slips during the large Mexican SSEs that occur every 4–5 years, which we refer to as the transient zone [e.g., *Kostoglodov et al.*, 2003; *Larson et al.*, 2007; *Radiguet et al.*, 2012]. The evolution of LFE activity in time and space is distinct in the transient zone: the activity is organized into large episodes of LFE activity that last several days long with little to no activity between the episodes. The stark contrast between the sweet spot and the transient zone is highlighted in Figure 6. The most significant amount of transient zone activity is observed during the 2006 SSE: over 4 months or so, there are clusters of LFEs every 5–10 days. Figure 8 shows a zoom of Figure 6 during the 2006 SSE. Following this logic, we reach the same conclusion as *Husker et al.* [2012], *Vergnolle et al.* [2010], and *Rivet et al.* [2014] and suggest that the six non-SSE LFE episodes associated with strong activity in the transient zone represent small short-term SSEs. Supposing slip rates similar to the large SSEs, the short duration of several days of small SSEs would not be long enough to accumulate enough slip to be above the noise level of GPS records. We speculate, however, that once higher precision measurements of slip are achieved, such as strain measured by tiltmeters, small short-term SSEs might become be geodetically observable.

Between the sweet spot and the transient zone, we observe an intermediate buffer zone. Activity within the sweet spot during LFE episodes extends into the buffer zone; outside of LFE episodes, however, there is little activity within the buffer zone. Whether this zone represents a stress barrier that must be overcome before the transient zone can slip is still a question that needs to be answered with further studies.

The near-constant occurrence of LFE clusters within the sweet spot reflects the near-constant slip rate in that zone; farther updip in the transient zone, however, the slip occurs in discrete episodes. This evolution of slip behavior, which has been observed in other subduction zones using tremor, has been suggested to represent the progression of frictional regimes, from brittle to ductile sliding [e.g., *Wech and Creager*, 2011]. We remind the reader, however, that unlike other subduction zones, the entirety of the LFE source region is located at more or less the same depth along the subhorizontal portion of the Cocos subduction, although

slowly increasing temperatures with increasing distance from the trench is expected along the interface due to slab cooling [*Manea and Manea*, 2011]. This along with the incredibly uniform distribution of LFE amplitudes along dip suggests that any differences in LFE activity do not reflect differences in the size of the LFE sources but instead reflect the evolution of the frictional properties of the interface. We suggest that pore pressure is primarily responsible for the drastic difference in LFE activity between the sweet spot and the transient zone. We do not think, however, that the observed migrations of LFE activity reflect the movement of fluid and instead propose that high pore pressures decrease the effective stress along the interface, facilitating faulting [*Wech and Creager*, 2011]. This study is not the first to have suggested that fluids along the fault interface play a large role in facilitating slow earthquakes [e.g., *Obara*, 2002; *Katsumata and Kamaya*, 2003; *Rogers and Dragert*, 2003; *Liu and Rice*, 2005; *Shelly et al.*, 2006; *Segall et al.*, 2010], but given the similar conditions of the two LFE source regions, we suggest that in Guerrero, Mexico, fluids are far and away the most important factor in determining the frictional regime of the subduction interface as it transitions from brittle to ductile.

6. Conclusions

We have generated a rich catalog of LFE activity in Guerrero, Mexico, by separating the detection process into two steps: (1) template detection and (2) multiplet detection. We emphasize the importance of the template detection to ensure that the matched-filter search used during the multiplet detection step searches for the largest number of different LFE sources possible. Simple, empirical statistics were then developed to select and regroup the 1120 LFE sources among the characterized event families. By sorting the catalog into subcatalogs representing the two principal LFE source regions in Guerrero, Mexico, the transient zone and the sweet spot, we observe distinct differences in LFE activity spatially and temporally: the sweet spot is characterized by clusters of LFEs distributed almost continuously in time with no apparent increase of activity during the large 2006 SSE; the transient zone's activity, on the other hand, is concentrated principally within the 2006 SSE and six other large episodes of activity that each last several days. The simple, but robust recipe presented here to generate a rich catalog of LFEs can be applied to other slow earthquake regions to extract precise information about LFEs and their evolution in time and space that wouldn't be possible otherwise without a continuous application of systematic LFE detection algorithms.

Acknowledgments

This study's generated catalog is available upon request to the corresponding author. We thank Aldo Zollo and Claudio Satriano for their program that was used to calculate the theoretical traveltimes. This work was supported by the Agence Nationale de la Recherche (France) under the contract RA0000CO69 (G-GAP) and by the European Research Council under the contract FP7 ERC Advanced grant 227507 (WHISPER). N. M. S. was supported by the Russian Science Foundation (grant 14-47-00002). Finally, one figure was made with Generic Mapping Tools [*Wessel and Smith*, 1998].

References

Aso, N., K. Ohta, and S. Ide (2013), Tectonic, volcanic, and semi-volcanic deep low-frequency earthquakes in western Japan, *Tectonophysics*, *600*, 26–40, doi:10.1016/j.tecto.2012.12.015.

Beroza, G. C., and S. Ide (2011), Slow earthquakes and nonvolcanic tremor, *Annu. Rev. Earth Planet. Sci.*, *39*, 271–296, doi:10.1146/annurev-earth-040809-152531.

Bostock, M. G., A. A. Royer, E. H. Hearn, and S. M. Peacock (2012), Low frequency earthquakes below southern Vancouver Island, *Geochem. Geophys. Geosyst.*, *13*, Q11007, doi:10.1029/2012GC004391.

Brown, J. R., G. C. Beroza, and D. R. Shelly (2008), An autocorrelation method to detect low frequency earthquakes within tremor, *Geophys. Res. Lett.*, *35*, L16305, doi:10.1029/2008GL034560.

Brown, J. R., G. C. Beroza, S. Ide, K. Ohta, D. R. Shelly, S. Y. Schwartz, W. Rabbel, M. Thorwart, and H. Kao (2009), Deep low-frequency earthquakes in tremor localize to the plate interface in multiple subduction zones, *Geophys. Res. Lett.*, *36*, L19306, doi:10.1029/2009GL040027.

Brown, J. R., S. G. Prejean, G. C. Beroza, J. S. Gomberg, and P. J. Haeussler (2013), Deep low-frequency earthquakes in tectonic tremor along the Alaska-Aleutian subduction zone, *J. Geophys. Res. Solid Earth*, *118*, 1079–1090, doi:10.1029/2012JB009459.

Caltech (2007), Meso-America Subduction Experiment (MASE) dataset, doi:10.7909/C3RN35SP.

Chamberlain, C. J., D. R. Shelly, J. Townend, and T. A. Stern (2014), Low-frequency earthquakes reveal punctuated slow slip on the deep extent of the Alpine Fault, New Zealand, *Geochem. Geophys. Geosyst.*, *15*, 2984–2999, doi:10.1002/2014GC005436.

Frank, W. B., and N. M. Shapiro (2014), Automatic detection of low-frequency earthquakes (LFEs) based on a beamformed network response, *Geophys. J. Int.*, *197*(2), 1215–1223, doi:10.1093/gji/ggu058.

Frank, W. B., N. M. Shapiro, V. Kostoglodov, A. L. Husker, M. Campillo, J. S. Payero, and G. A. Prieto (2013), Low-frequency earthquakes in the Mexican sweet spot, *Geophys. Res. Lett.*, *40*, 2661–2666, doi:10.1002/grl.50561.

Ghosh, A., J. E. Vidale, J. R. Sweet, K. C. Creager, A. G. Wech, H. Houston, and E. E. Brodsky (2010), Rapid, continuous streaking of tremor in Cascadia, *Geochem. Geophys. Geosyst.*, *11*, Q12010, doi:10.1029/2010GC003305.

Gibbons, S. J., and F. Ringdal (2006), The detection of low magnitude seismic events using array-based waveform correlation, *Geophys. J. Int.*, *165*(1), 149–166, doi:10.1111/j.1365-246X.2006.02865.x.

Husker, A. L., V. Kostoglodov, V. M. Cruz-Atienza, D. Legrand, N. M. Shapiro, J. S. Payero, M. Campillo, and E. Huesca-Pérez (2012), Temporal variations of non-volcanic tremor (NVT) locations in the Mexican subduction zone: Finding the NVT sweet spot, *Geochem. Geophys. Geosyst.*, *13*, Q03011, doi:10.1029/2011GC003916.

Iglesias, A., R. W. Clayton, X. Pérez-Campos, S. K. Singh, J. F. Pacheco, D. García, and C. Valdés-González (2010), S wave velocity structure below central Mexico using high-resolution surface wave tomography, *J. Geophys. Res.*, *115*, B06307, doi:10.1029/2009JB006332.

Katsumata, A., and N. Kamaya (2003), Low-frequency continuous tremor around the Moho discontinuity away from volcanoes in the southwest Japan, *Geophys. Res. Lett.*, *30*(1), 1020, doi:10.1029/2002GL015981.

Kim, Y., R. W. Clayton, and J. M. Jackson (2010), Geometry and seismic properties of the subducting Cocos plate in central Mexico, *J. Geophys. Res.*, *115*, B06310, doi:10.1029/2009JB006942.
Kostoglodov, V., and J. F. Pacheco (1999), Cien años de sismicidad en México, Instituto de Geofísica, Universidad Nacional Autónoma de México. [Available at http://usuarios.geofisica.unam.mx/vladimir/sismos/100a%F1os.html.]
Kostoglodov, V., S. K. Singh, J. A. Santiago, S. I. Franco-Sanchez, K. M. Larson, A. R. Lowry, and R. G. Bilham (2003), A large silent earthquake in the Guerrero seismic gap, Mexico, *Geophys. Res. Lett.*, *30*(15), 1807, doi:10.1029/2003GL017219.
Kostoglodov, V., A. L. Husker, N. M. Shapiro, J. S. Payero, M. Campillo, N. Cotte, and R. W. Clayton (2010), The 2006 slow slip event and nonvolcanic tremor in the Mexican subduction zone, *Geophys. Res. Lett.*, *37*, L24301, doi:10.1029/2010GL045424.
Larson, K. M., V. Kostoglodov, S. Miyazaki, and J. A. Santiago (2007), The 2006 aseismic slow slip event in Guerrero, Mexico: New results from GPS, *Geophys. Res. Lett.*, *34*, L13309, doi:10.1029/2007GL029912.
Liu, Y., and J. R. Rice (2005), Aseismic slip transients emerge spontaneously in three-dimensional rate and state modeling of subduction earthquake sequences, *J. Geophys. Res.*, *110*, B08307, doi:10.1029/2004JB003424.
Manea, V. C., and M. Manea (2011), Flat-slab thermal structure and evolution beneath Central Mexico, *Pure Appl. Geophys.*, *168*(8–9), 1475–1487, doi:10.1007/s00024-010-0207-9.
Obara, K. (2002), Nonvolcanic deep tremor associated with subduction in southwest Japan, *Science*, *296*(5573), 1679–1681.
Obara, K., S. Tanaka, T. Maeda, and T. Matsuzawa (2010), Depth-dependent activity of non-volcanic tremor in southwest Japan, *Geophys. Res. Lett.*, *37*, L13306, doi:10.1029/2010GL043679.
Payero, J. S., V. Kostoglodov, N. M. Shapiro, T. Mikumo, A. Iglesias, X. Pérez-Campos, and R. W. Clayton (2008), Nonvolcanic tremor observed in the Mexican subduction zone, *Geophys. Res. Lett.*, *35*, L07305, doi:10.1029/2007GL032877.
Pérez-Campos, X., Y. Kim, A. L. Husker, P. M. Davis, R. W. Clayton, A. Iglesias, J. F. Pacheco, S. K. Singh, V. C. Manea, and M. Gurnis (2008), Horizontal subduction and truncation of the Cocos Plate beneath central Mexico, *Geophys. Res. Lett.*, *35*, L18303, doi:10.1029/2008GL035127.
Radiguet, M., F. Cotton, M. Vergnolle, M. Campillo, B. Valette, V. Kostoglodov, and N. Cotte (2011), Spatial and temporal evolution of a long term slow slip event: The 2006 Guerrero slow slip event, *Geophys. J. Int.*, *184*(2), 816–828, doi:10.1111/j.1365-246X.2010.04866.x.
Radiguet, M., F. Cotton, M. Vergnolle, M. Campillo, A. Walpersdorf, N. Cotte, and V. Kostoglodov (2012), Slow slip events and strain accumulation in the Guerrero gap, Mexico, *J. Geophys. Res.*, *117*, B04305, doi:10.1029/2011JB008801.
Rivet, D., et al. (2014), Seismic velocity changes, strain rate and non-volcanic tremors during the 2009–2010 slow slip event in Guerrero, Mexico, *Geophys. J. Int.*, *196*, 447–460, doi:10.1093/gji/ggt374.
Rogers, G., and H. Dragert (2003), Episodic tremor and slip on the Cascadia subduction zone: The chatter of silent slip, *Science*, *300*(5627), 1942–1943, doi:10.1126/science.1084783.
Royer, A. A., and M. G. Bostock (2013), A comparative study of low frequency earthquake templates in Northern Cascadia, *Earth Planet. Sci. Lett.*, *402*, 247–256, doi:10.1016/j.epsl.2013.08.040.
Schwartz, S. Y., and J. M. Rokosky (2007), Slow slip events and seismic tremor at circum-Pacific subduction zones, *Rev. Geophys.*, *45*, RG3004, doi:10.1029/2006RG000208.
Segall, P., A. M. Rubin, A. M. Bradley, and J. R. Rice (2010), Dilatant strengthening as a mechanism for slow slip events, *J. Geophys. Res.*, *115*, B12305, doi:10.1029/2010JB007449.
Shelly, D. R. (2009), Possible deep fault slip preceding the 2004 Parkfield earthquake, inferred from detailed observations of tectonic tremor, *Geophys. Res. Lett.*, *36*, L17318, doi:10.1029/2009GL039589.
Shelly, D. R. (2010), Periodic, chaotic, and doubled earthquake recurrence intervals on the deep San Andreas Fault, *Science*, *328*(5984), 1385–1388, doi:10.1126/science.1189741.
Shelly, D. R., G. C. Beroza, S. Ide, and S. Nakamula (2006), Low-frequency earthquakes in Shikoku, Japan, and their relationship to episodic tremor and slip, *Nature*, *442*(7099), 188–191, doi:10.1038/nature04931.
Shelly, D. R., G. C. Beroza, and S. Ide (2007a), Non-volcanic tremor and low-frequency earthquake swarms, *Nature*, *446*(7133), 305–307, doi:10.1038/nature05666.
Shelly, D. R., G. C. Beroza, and S. Ide (2007b), Complex evolution of transient slip derived from precise tremor locations in western Shikoku, Japan, *Geochem. Geophys. Geosyst.*, *8*, Q10014, doi:10.1029/2007GC001640.
Tang, C. C., Z. Peng, K. Chao, C. H. Chen, and C.-H. Lin (2010), Detecting low-frequency earthquakes within non-volcanic tremor in southern Taiwan triggered by the 2005 Mw 8.6 Nias earthquake, *Geophys. Res. Lett.*, *37*, L16307, doi:10.1029/2010GL043918.
Vergnolle, M., A. Walpersdorf, V. Kostoglodov, P. Tregoning, J. A. Santiago, N. Cotte, and S. I. Franco-Sanchez (2010), Slow slip events in Mexico revised from the processing of 11 year GPS observations, *J. Geophys. Res.*, *115*, B08403, doi:10.1029/2009JB006852.
Wech, A. G., and K. C. Creager (2011), A continuum of stress, strength and slip in the Cascadia subduction zone, *Nat. Geosci.*, *4*(7), 624–628, doi:10.1038/ngeo1215.
Wessel, P., and W. H. F. Smith (1998), New, improved version of generic mapping tools released, *Eos Trans. AGU*, *79*(47), 579–579, doi:10.1029/98EO00426.